Redox Biology 69 (2024) 103007

Contents lists available at ScienceDirect

Redox Biology

journal homepage: www.elsevier.com/locate/redox

Inhibiting the compensatory elevation of xCT collaborates with disulfiram/copper-induced GSH consumption for cascade ferroptosis and cuproptosis

Ping Zhang [a,b,1], Chaoting Zhou [b,1], Xueying Ren [c,1], Qiangan Jing [a], Yan Gao [a], Chen Yang [a], Yuhuan Shen [a], Yi Zhou [a], Wanye Hu [d], Feifan Jin [a], Haifeng Xu [a], Lingyan Yu [a], Yingchao Liu [a], Xiangmin Tong [a,b,**], Yanchun Li [b,***], Ying Wang [a,b,****], Jing Du [a,*]

[a] Laboratory Medicine Center, Department of Clinical Laboratory, Zhejiang Provincial People's Hospital(Affiliated People's Hospital), Hangzhou Medical College, Hangzhou, Zhejiang, China
[b] Department of Central Laboratory, Affiliated Hangzhou First People's Hospital, School of Medicine, Westlake University, Hangzhou, Zhejiang, China
[c] Department of Clinical Laboratory, The Second Affiliated Hospital of Zhejiang Chinese Medical University, Hangzhou, Zhejiang, China
[d] Department of Clinical Laboratory, The Second Affiliated Hospital of Soochow University, Suzhou, Jiangsu, China

ARTICLE INFO

Keywords:
Hepatocellular carcinoma
DSF/Cu
Ferroptosis
Cuproptosis
xCT

ABSTRACT

Hepatocellular carcinoma (HCC) is one of the most prevalent malignant tumors and the fourth leading cause of cancer-related death globally, which is characterized by complicated pathophysiology, high recurrence rate, and poor prognosis. Our previous study has demonstrated that disulfiram (DSF)/Cu could be repurposed for the treatment of HCC by inducing ferroptosis. However, the effectiveness of DSF/Cu may be compromised by compensatory mechanisms that weaken its sensitivity. The mechanisms underlying these compensatory responses are currently unknown. Herein, we found DSF/Cu induces endoplasmic reticulum stress with disrupted ER structures, increased Ca^{2+} level and activated expression of ATF4. Further studies verified that DSF/Cu induces both ferroptosis and cuproptosis, accompanied by the depletion of GSH, elevation of lipid peroxides, and compensatory increase of xCT. Comparing ferroptosis and cuproptosis, it is interesting to note that GSH acts at the crossing point of the regulation network and therefore, we hypothesized that compensatory elevation of xCT may be a key aspect of the therapeutic target. Mechanically, knockdown of ATF4 facilitated the DSF/Cu-induced cell death and exacerbated the generation of lipid peroxides under the challenge of DSF/Cu. However, ATF4 knockdown was unable to block the compensatory elevation of xCT and the GSH reduction. Notably, we found that DSF/Cu induced the accumulation of ubiquitinated proteins, promoted the half-life of xCT protein, and dramatically dampened the ubiquitination–proteasome mediated degradation of xCT. Moreover, both pharmacologically and genetically suppressing xCT exacerbated DSF/Cu-induced cell death. In conclusion, the current work provides an in-depth study of the mechanism of DSF/Cu-induced cell death and describes a framework for the further understanding of the crosstalk between ferroptosis and cuproptosis. Inhibiting the compensatory increase of xCT renders HCC cells more susceptible to DSF/Cu, which may provide a promising synergistic strategy to sensitize tumor therapy and overcome drug resistance, as it activates different programmed cell death.

* Corresponding author. Laboratory Medicine Center, Department of Clinical Laboratory, Zhejiang Provincial People's Hospital(Affiliated People's Hospital), Hangzhou Medical College, Hangzhou, Zhejiang, China.
** Corresponding author. Department of Central Laboratory, Affiliated Hangzhou First People's Hospital, School of Medicine, Westlake University, Hangzhou, Zhejiang, China.
*** Corresponding author. Department of Central Laboratory, Affiliated Hangzhou First People's Hospital, School of Medicine, Westlake University, Hangzhou, Zhejiang, China.
**** Corresponding author. Department of Central Laboratory, Affiliated Hangzhou First People's Hospital, School of Medicine, Westlake University, Hangzhou, Zhejiang, China.
E-mail addresses: tongxiangmin@163.com (X. Tong), lycmed@163.com (Y. Li), nancywangying@163.com (Y. Wang), dujing1@hmc.edu.com (J. Du).
[1] These authors contributed equally to this work.

https://doi.org/10.1016/j.redox.2023.103007
Received 24 November 2023; Received in revised form 17 December 2023; Accepted 18 December 2023
Available online 19 December 2023

1. Introduction

Hepatocellular carcinoma (HCC) is an invasive type of cancer with increasing incidences and mortality rates, particularly in East Asia and Africa [1]. The 5-year survival rate of HCC patients is still below 20 % leading to a poor outcome, which is still a global health challenge [2]. The stage of the tumor greatly influences the prognosis. Early HCC patients' treatment includes liver transplantation, surgical resection, and locoregional therapies, but unfortunately, most patients are diagnosed at an advanced stage [3]. Conventional cancer chemotherapeutics such as paclitaxel and cisplatin have limited effectiveness in HCC [4]. Currently, the FDA-approved chemotherapeutics for the treatment of HCC involve tyrosine kinase inhibitors sorafenib and lenvatinib [5,6]. However, the acquired drug resistance of tyrosine kinase inhibitors exhibits certain limitations for the treatment of HCC [7]. Therefore, it is urgent to discover novel and effective drugs for HCC treatment.

The time and capital cost of new drug research confer it with great risks, thus drug repurposing is a fast and low-cost approach [8]. Disulfiram (DSF) is an acetaldehyde dehydrogenase inhibitor approved by FDA in 1951 to treat chronic alcohol addiction. Previous research has reported that DSF could be metabolized into diethyldithiocarbamate (DTC) by the disulfide fragmentation at the center of symmetric structure, and then DTC combines with Cu to form the DTC-Cu complex (CuET) [9,10]. CuET is a Cu (II) diethyldithiocarbamate complex, serves as the primary component responsible for the anti-tumor effect of DSF/Cu [11]. Further studies proved that DSF/Cu can induce the death of various tumor cells such as breast cancer cells [12], non-small cells [13], lung cancer cells [14], esophageal cancer cells [15], meningioma cells [16], and mesothelioma cells [17]. For HCC, DSF/Cu was found to inhibit metastasis by NF-κB and TGF-β pathways [18]. Moreover, our previous study indicated that DSF/Cu could disrupt mitochondrial homeostasis, increase free iron, and exert an important role of ferroptosis in DSF/Cu-caused cell death [19].

Ferroptosis is a new programmed cell death first discovered in 2012, indivisibly linked with lipid peroxide accumulation [20]. The major molecular pathways of ferroptosis are iron metabolism, GPX4/GSH, NRF2, System Xc^-, mitochondrial metabolism, and FSP1-CoQ10 [21–23]. Several drugs, such as sorafenib, sunitinib, zalcitabine, dihydroartemisinin, and cetuximab, have been identified as implicated in the regulation of ferroptotic cell death and increased sensitivity of cancer cells to conventional therapy [24–27]. In HCC, targeting ferroptosis is verified significantly improve the therapeutic effect of HCC by reducing the drug resistance of HCC cells to sorafenib [28,29]. Therefore, inducing ferroptosis is a promising therapeutic strategy.

Endoplasmic reticulum (ER) is a key organelle that maintains intracellular homeostasis, participates in protein folding, assembly, transport, and maintains the homeostasis of intracellular calcium levels [30]. Whereas, various exogenous factors, such as hypoxia and oxidative stress, easily cause unfolded protein response (UPR) in ER, and lead to ER stress [31]. The UPR serves as an adaptive response and endogenous protective mechanism in response to cellular stimuli. It transmits stress signals from the ER to the nucleus, ultimately restoring ER homeostasis through mechanisms such as reducing protein synthesis, facilitating proper protein folding, and enhancing the degradation of misfolded or unfolded proteins [32,33]. Emerging evidence indicated ER stress response is activated synchronously during the initiation of ferroptosis [34]. PERK-eIF2α-ATF4 signal pathway was capable of ameliorating ferroptosis by up-regulating HSPA5 and System Xc^- [35,36]. On the other hand, erastin-induced ER stress activates the PERK-eIF2α-ATF4-CHOP pathway, leading to an increase in PUMA expression, which participates in the regulation of ferroptosis [37].

In our study, we aimed to explore the specific mechanism of DSF/Cu in HCC. It is found that DSF/Cu induces ER stress, as evidenced by the expanded ER, increased Ca^{2+} level and activated expression of ATF4. Further studies verified that DSF/Cu induces both ferroptosis and cuproptosis, which is accompanied by the depletion of GSH, elevation of lipid peroxides, and compensatory elevation of xCT. Remarkably, our finding indicated that xCT expression was elevated through the inhibition of ubiquitination–proteasome mediated degradation rather than ATF4-dependent transactivation [38]. Suppressing the compensatory increase of xCT facilitated the sensitivity of HCC to DSF/Cu-induced cell death. In conclusion, these results provide evidence that DSF/Cu may induce multiple forms of cell death simultaneously, and suppressing the elevated xCT strengthens HCC cells more vulnerable to DSF/Cu.

2. Materials and methods

2.1. Reagents and antibodies

DSF and Cu were freshly mixed at a l:l ratio and used in the *in vitro* experiments. Enhanced Cell Counting Kit-8 (CCK-8 kit), Calcein/PI kit, EdU assay kit, Hoechst 33342, ER-Tracker Red and Fluo-4 AM were acquired from Beyotime (Shanghai, China). DCF-DA and C11-BODIPY (581/591) were purchased from Thermo Fisher Scientific (Waltham, MA). Disulfiram (DSF), $CuCl_2$, Monochlorobimane (MCB), Tauroursodeoxycholic acid (TUDCA), Deferoxamine (DFO), Tetrathiomolybdate (TTM), Bathocuproine disulfonic acid (BCS), Glutathione (GSH), Cycloheximide (CHX) and MG132 were purchased from Sigma-Aldrich (St. Louis, MO, USA). Salicylazosulfapyridine (SASP), Erastin, Z-VAD-FMK, Necrosuifonamide (Necro), and Bafilomycin A1 (Baf-A1) were obtained from Selleck Chemicals (Houston, TX). The antibodies to GAPDH (ab8245), β-Actin (ab8226), p-eIF2α (ab32157), HSP70 (ab194360), NRF2 (ab62352), xCT (ab175186), FTH (ab75973), CSE (ab189916), GPX4 (ab125066), Glutaminase (ab156876), Glucose transporter 1 (GluT1) (ab115730), Recombinant Glutathione Reductase 1 (GRD1) (ab124995), Ki-67 (ab15580), ATP7B (ab124973), NFS1 (ab197253) and NDUFV2 (ab183717) were purchased from Abcam. eIF2α (11170-1-AP), ATF4 (10835-1-AP), CHOP (15204-1-AP), IRE1 (27528-1-AP) FDX1 (12592-1-AP) and Ubiquitination (23516-1-AP) were purchased from Proteintech. CBS (A11612) were purchased from ABClonal. GAPDH and β-Actin antibodies were used with 4000-fold dilution and other antibodies were used with 1000-fold dilution.

2.2. Cell culture

SMMC-7721, Huh7 and 293T cells were preserved and passaged in our laboratory and cultured in a DMEM medium (Gibco, USA) containing 10 % fetal bovine serum (Gibco, USA) and 1 % penicillin-streptomycin in a cell culture incubator which was kept at the temperature of 37 °C and 5 % CO_2 with humidification. All experiments were performed using cells with more than 90 % viability in the logarithmic phase of growth.

2.3. CCK-8 assay

CCK-8 was utilized to evaluate cell viability which consists of tetrazolium salts that react with dehydrogenase in cells to produce yellow formazan dye [39]. Firstly, cells were plated on 96-well plates with a density of 8,000 cells per well, cultured in DMEM medium involving 10 % fetal bovine serum for the night. Then, the medium was replaced with a DMEM medium containing various drug concentrations to culture cells for 12 h. Before measuring at 450 nm using a microplate reader (Thermo Fisher), 10 μL CCK-8 was added to each well and incubated for 2 h at 37 °C.

2.4. Lentiviral packaging and transduction

The expression of ATF4 and xCT were silenced using pLVX-shRNA Lentivector (Takara, Japan) according to our previous publication [40]. The shRNA knockdown sequences are shown in Table S1 xCT cDNA was obtained from Sino Biological (Beijing, China) and subcloned into a pLVX-IRES-Neo lentivirus vector (Takara, Japan). The

recombinant lentiviral plasmids were verified by sequencing and co-transfected with PMD2.G and PSPAX2 in 293T cells for lentiviral packaging. Then the supernatants were collected and filtered through a 0.45 μm filter. SMMC-7721 and Huh7 cells were plated in a 24-well plate overnight and transfected with the corresponding lentivirus for 2 days. Next, 1 mg/mL G418 or 2 μg/mL puromycin was added for the selection of stably transfected cell lines.

2.5. EdU assay

The 5-ethynyl-2-deoxyuridine (EdU) is a pyrimidine analog that can be integrated into DNA double-strand during DNA synthesis [41]. EdU assay was performed to detect the cell proliferation capacity of SMMC-7721 and Huh7 cells treated with or without DSF/Cu. Images were captured by confocal microscopy.

2.6. Live/dead cell staining assay

SMMC-7721 and Huh7 cells (8×10^4) were seeded in a confocal dish (NEST Biotechnology). DSF/Cu (0–1 μM) was added into the indicated wells for 12 h. Then, the cells were incubated with Calcein-AM and PI for the staining of live and dead cells. Nuclei were also counterstained with Hoechst 33342 (1 μg/mL) for 10 min. The fluorescence was observed under a confocal microscope (Leica TCS SP5, German).

2.7. Confocal microscopy assay

The cells were plated in a confocal dish for 12 h. After the treatment of DSF/Cu, the cells were stained with different probes, including C11-BODIPY (4 μM), ER-Tracker Red (0.5 μM), Fluo-4 AM (1 μM), MCB (25 μM), for 30 min. Meanwhile, the cells were co-stained with Hoechst 33342 (1 μg/mL). Then the stained cells were washed with PBS three times and visualized under laser confocal microscopy.

2.8. Real-time PCR (RT-PCR)

The total RNA from the treated HCC cells was extracted by the AG RNAex Pro Reagent (Accurate Biology). Afterward, RNA was reversed into cDNA utilizing Evo M-MLVRT Kit (Accurate Biology) according to the instructions. Gene expression was quantified by SYBR Green base RT-PCR and normalized to the level of the housekeeping gene. The primers of quantitative real-time PCR are shown in Table S2.

2.9. Western blot assay

After being treated with drugs, cells were lysed by scraping in RIPA buffer. Supernatants including total cellular proteins were obtained following centrifugation. Proteins were quantified by the BCA Protein Assay Kit (Boxbio Science & Technology, Beijing), and were separated by 10 % SDS-PAGE. Subsequently, proteins were transferred onto the PVDF membrane (Bio-Rad) and blocked with 5 % non-fat milk. The membranes were incubated with the corresponding primary antibody at 4 °C for at least 8 h. After being washed by TBST three times, the membranes were incubated with HRP-conjugated anti-rabbit or anti-mouse antibodies for 1 h. Finally, proteins were visualized by a Fdbio-Plco ECL kit (Fdbio science) in an enhanced chemiluminescence system (Bio-Rad, United States). ImageJ was used to quantify the band intensities.

2.10. CoIP assay

CoIP assay was performed using the Capturem™ IP&COIP kit (TaKaRa, Japan) according to the manufacturer's instructions. Huh7 cells with xCT over-expression were lysed on ice by cell lysis buffer for 15 min and centrifuged at 4 °C for 10 min. The lysed proteins were incubated with the corresponding antibody overnight at 4 °C under constant mixing. After washings in the column, antibody-protein complexes were eluted with 40 μl of Elution Buffer and subjected to WB analysis.

2.11. Animal experiments

The animal experiments were approved by the ethics committee of Zhejiang Provincial People's Hospital. Six-week-old BALB/c nude mice were purchased from the Shanghai Laboratory Animal Center and fed under SPF conditions. Huh7 cells were collected and resuspended in DMEM medium at a concentration of 2×10^7/mL. The right flank of each BALB/c nude mouse was injected subcutaneously with 0.2 mL of the Huh7 cell suspension. The animals were randomly divided into the Control group and DSF/Cu-treated group when the tumor reached 100–200 mm^3. In the DSF/Cu-treated group, $CuCl_2$ (0.06 mg/kg) was injected intramuscularly and 50 mg/kg DSF was taken intraperitoneally 2 h later. The mice's tumor volume was measured every 3 days. At the end of the experiments, the mice were euthanized by CO_2 inhalation. The blood samples were collected for safety assessment, and the tumors and organs were removed and collected.

2.12. Hematoxylin-eosin (H&E) and immunohistochemistry staining

Tumor samples obtained from mice were fixed with 4 % paraformaldehyde (Leagene Biotechnology, China), embedded into the paraffin and cut into 4 μm thick sections. The tissue sections were performed with routine hematoxylin and eosin (H&E) staining. The immunohistochemistry assay was carried out after dewaxed, hydrated and antigen retrieval. The endogenous peroxidases were inactivated with 3 % peroxide and the sections were blocked with 5 % BSA. Ki-67 antibody was used with 100-fold dilution. Subsequently, the sections were incubated with normal rabbit IgG (Beyotime, China) for 30 min and added with horseradish for 15 min. The stained sections both were viewed and photographed under a microscope.

2.13. Statistical analysis

All statistical calculations were performed using GraphPad Prism (version 9.0). Results are represented as mean ± SD. The differences between the two groups were performed by the student's *t*-test. Comparisons among multiple groups were analyzed by one-way ANOVA. Statistical significance was defined as * $P < 0.05$, ** $P < 0.01$, *** $P < 0.001$.

3. Results

3.1. DSF/Cu inhibits cell viability and proliferation of HCC cells

Our and other previous studies have shown that DSF/Cu exerts preferential toxicity toward HCC cells while sparing lower toxicity toward the non-malignant cells [10,42]. By comparing the toxic effects of DSF and $CuCl_2$ alone and in combination, the results revealed that the anticancer effect of DSF in HCC cells was copper-dependent (Figs. S1A–B). To further verify the antitumor activity of DSF/Cu in HCC cells, the Calcein-AM/PI staining was utilized to calculate the percentage of live (Calcein-AM^+/PI^-) and dead (Calcein-AM^-/PI^+) cells. The results showed that the amounts of dead cells increased with the increase of DSF/Cu concentration, while the live cells characterized as calcein positive were reduced significantly, indicating that DSF/Cu accelerated cell death of HCC cells (Fig. 1A and B). We then tested whether the administration of DSF/Cu could suppress the cell proliferation of HCC cells. As expected, the results of the EdU incorporation assay revealed that DSF/Cu significantly disrupted the growth of HCC cells, evidenced by the significant decrease of EdU-positive cells (Fig. 1C–F). Taken together, these results showed that DSF/Cu could inhibit the viability and suppress the proliferation of HCC cells.

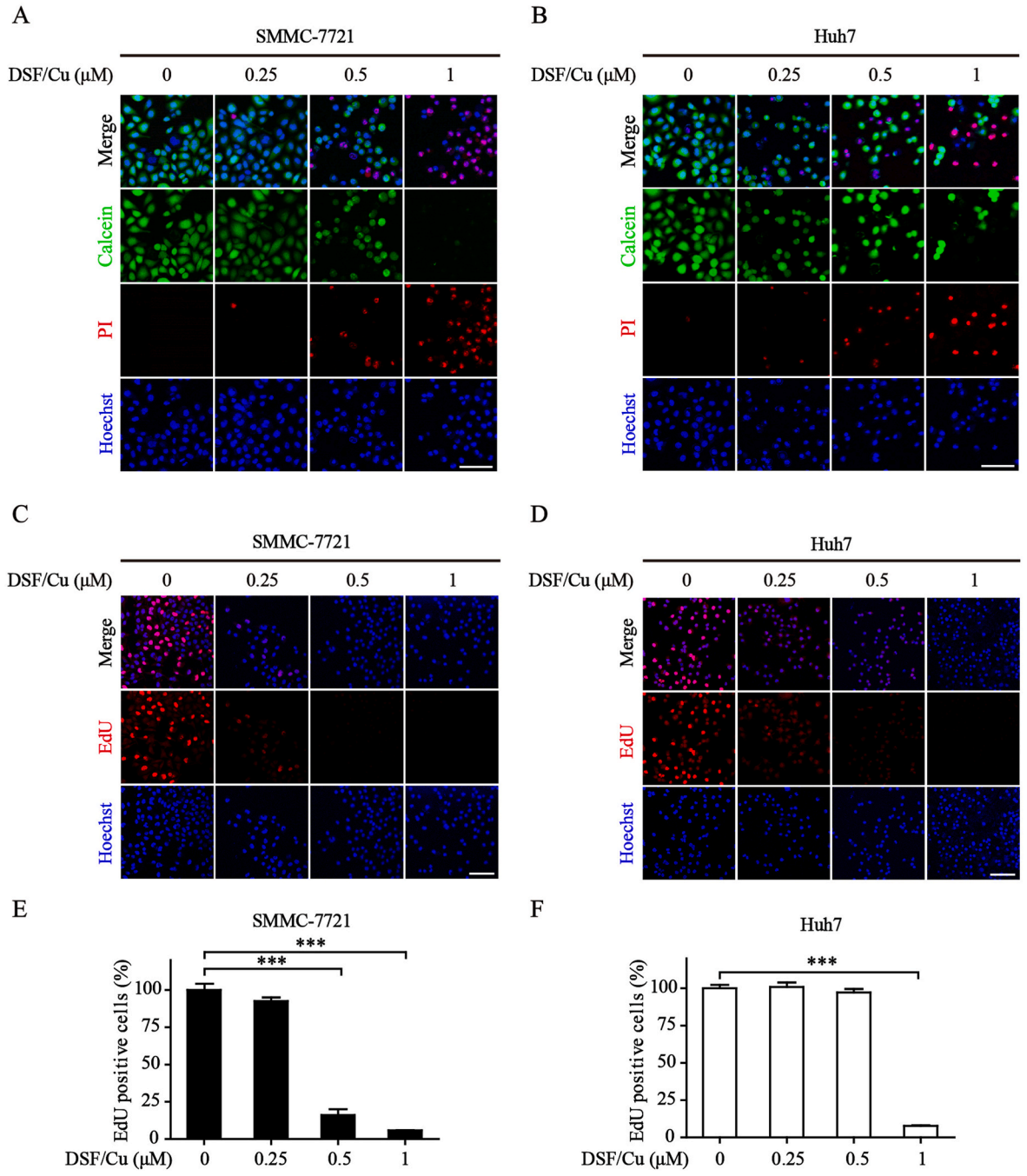

Fig. 1. The cytotoxic effects of DSF/Cu on HCC cells
(A, B) The cytotoxicity of SMMC-7721 and Huh7 were detected by Calcein/PI assay under treatment of DSF/Cu (0–1 μM) for 12 h. Green fluorescence is marked with living cells stained by Calcein, and red fluorescence is marked with dead cells stained by PI. Scale bar: 100 μm. (C–F) Representative images of SMMC-7721 and Huh7 stained for 5-ethynyl-2′-deoxyuridine (EdU) after treatment of DSF/Cu (0–1 μM) for 12 h. Scale bar: 100 μm. The quantitative histograms were displayed below the images. (Compared with control, *** indicated $P < 0.001$). (For interpretation of the references to colour in this figure legend, the reader is referred to the Web version of this article.)

3.2. DSF/Cu induces endoplasmic reticulum stress in HCC cells

To gain insight into how DSF/Cu affects the function of HCC cells, the transcriptomes of DSF/Cu-treated and control cells were subjected to RNA-seq analysis. PCA analysis showed significant differences between the control and treated groups (Fig. S2A), and the Kyoto Encyclopedia of Genes and Genomes (KEGG) pathway analysis of differentially expressed genes (DEGs) between the two groups manifested that processes including ER function and ferroptosis were significantly enriched (Fig. S2B). We also performed gene-set enrichment analysis (GSEA) and found ER stress was highly activated in the DSF/Cu-treated cells (Fig. S2C). It is well known that the synthesis, folding and secretion of newly synthesized proteins are the essential functions of ER, which is tightly regulated to maintain the growth, survival and differentiation of cells [43]. We then explored whether DSF/Cu exerts an impact on ER homeostasis. Firstly, the morphology of ER was assessed by the staining of ER-membrane-specific probe ER-Tracker Red. Results from the laser confocal microscope showed that, compared to the network-like morphology in the control group, DSF/Cu treatments resulted in dilated, short ER structures with decreased ER area (Fig. 2A and B).

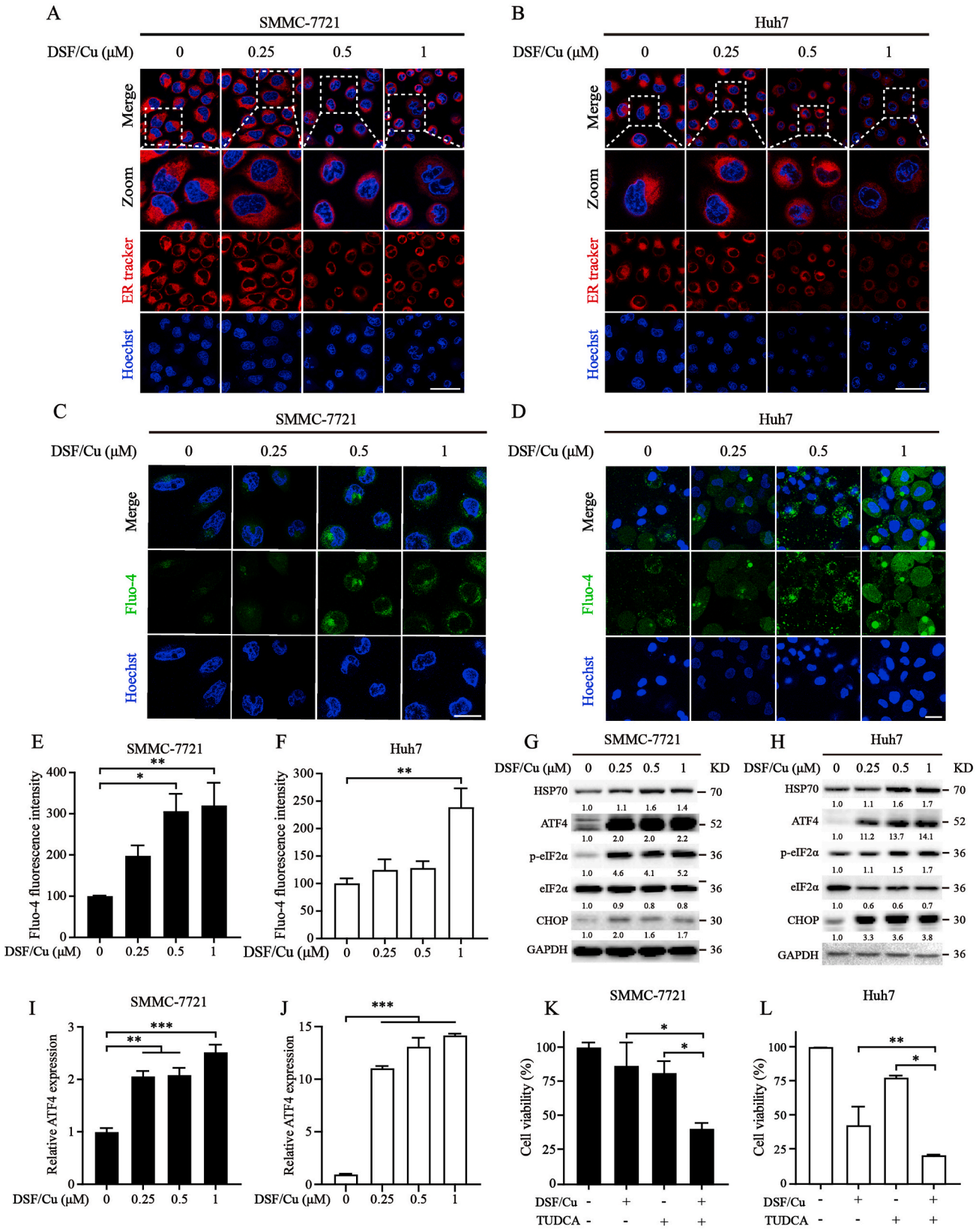

Fig. 2. DSF/Cu induces endoplasmic reticulum stress in HCC cells

(A, B) The morphological changes of the endoplasmic reticulum in SMMC-7721 and Huh7 with DSF/Cu (0–1 μM) treatment were monitored by ER tracker (0.5 μM). Scale bar: 50 μm. (C, D) SMMC-7721 and Huh7 under DSF/Cu (0–1 μM) treatment were stained with Fluo-4 AM (1 μM). probe and photographed by confocal laser microscope. Scale bar: 50 μm. The corresponding quantitative histograms were listed in (E) and (F), respectively. (G–J) Total protein was harvested from HCC cells that had been treated by DSF/Cu (0–1 μM), and western blot assay was performed to analyze ER stress-related proteins. (K, L) SMMC-7721 and Huh7 were exposed to DMSO or DSF/Cu for 12 h with or without TUDCA (1 mM). CCK-8 assay was applied to measure cell viability. (Compared with control, * indicated $P < 0.05$, ** indicated $P < 0.01$).

Given that ER is an important reservoir of intracellular calcium ion (Ca^{2+}) [44], we then detected calcium flux through the fluorescent probe Fluo-4 AM. We found that the fluorescence intensity of Fluo-4 AM increased significantly in SMMC-7721 and Huh7 cells under the treatment of DSF/Cu compared with the control cells, suggesting ER stress may occur (Fig. 2C–F). Therefore, several proteins associated with ER stress were detected by western blot. The results revealed that DSF/Cu treatment could increase the phosphorylation of eIF2α, and elevate the level of ATF4, HSP70 and CHOP in HCC cells (Fig. 2G–J). Moderate activation of ER stress attempts to support the restoration of ER homeostasis in response to the stress. Interestingly, inhibition of ER stress with TUDCA could strengthen the cell death induced by DSF/Cu, indicating ER stress may be a compensatory mechanism activated to weaken the toxicity of DSF/Cu (Fig. 2K and L). These data revealed that DSF/Cu induced ER stress in HCC cells and activated the expression of ATF4, which may act as a compensatory mechanism in damaged cells.

3.3. DSF/Cu induces compensatory activation of cellular xCT expression

Recently, researchers identified that copper ionophores, such as Elesclomol or DSF, could induce cuproptosis. The distinct form of regulated cell death is characterized by lipoylated protein aggregation and subsequent iron-sulfur cluster protein loss, while GSH is a well-characterized copper-binding ligand that could rapidly trap Cu^{+} in the stable Cu^{+}−GSH complex [45]. On the other hand, our previous study discovered that DSF/Cu efficiently induced ferroptotic cell death [19]. Comparing ferroptosis and cuproptosis, it is interesting to note that GSH acts at the crossing point of the regulation network and therefore, we hypothesized that GSH may be a key aspect of the therapeutic target. Subsequently, several cell death inhibitors were used in combination with DSF/Cu. As shown in Fig. 3A and B and Figs. S3A–C, the DSF/Cu-induced cell death was rescued by DFO (iron chelator), GSH, TTM and BCS (copper chelator), but hardly improved by Z-VAD-FMK (apoptosis inhibitor), Necro (necroptosis inhibitor) and Baf-A1 (autophagy inhibitor). DFO, TTM and GSH may act both inside and outside of cells, therefore these inhibitors were pretreated to the cells for a duration of 12 h, after which they were removed and the cells were subsequently treated with DSF/Cu alone. Consistent with the findings presented in Fig. 3A and B, it was observed that pretreatment with GSH, DFO, and TTM resulted in a mitigation of the toxicity induced by DSF/Cu (Fig. S3D). γ-GT (γ-glutamyl transpeptidase) is required for GSH to enter the cell. However, the activity of γ-GT is not significantly affected by DSF/Cu (Fig. S3E). Intriguingly, iron-sulfur cluster proteins decreased in HCC cells after DSF/Cu treatment, which is an important characteristic of cuproptosis (Fig. S4). Additionally, lipid peroxides were remarkably accumulated accompanied by a decrease in GSH, GSH/GSSG, total glutathione, and an increase in GSSG following DSF/Cu treatment (Fig. 3C–I and Figs. S3F–G). Furthermore, the pretreatment of DFO could restore the DSF/Cu-mediated decrease in GSH (Fig. 3G–I).

The transsulfuration pathway is an important way to generate GSH and H_2S, which includes two key enzymes: CBS and CSE. In the presence of CBS and CSE, cysteine undergoes a reaction with homocysteine to produce H_2S [46]. The western blot results revealed that the expression of CBS was upregulated. Previous research has demonstrated that ATF4 was the key regulator responsible for the transcriptional activation of CBS [47], which may be the potential mechanism for the upregulated of CBS under the treatment of DSF/Cu. The expression of CSE protein was diminished by DSF/Cu, consequently inhibiting the conversion of cystathionine to cysteine (Fig. S5A). Additionally, the heightened fluorescence intensity of WSP-1 indicated an increase in H_2S, suggesting that part of the cysteine is catalyzed to H_2S (Figs. S5B–C). Furthermore, the exact role of transsulfuration in DSF/Cu-induced cell death is an issue that merits further exploration.

On the other hand, western blot results indicated that DSF/Cu efficiently facilitated the degradation of GPX4 and ferritin heavy chain (FTH), thus leading to the catastrophic accumulation of free iron and unrestricted lipid peroxidation (Fig. 3J–K and Figs. S5D–E). Concomitantly, xCT and glutathione reductase 1 (GRD1) were compensatorily activated to maintain the GSH level and the key antioxidant transcription factor NRF2 was compensatorily increased to alleviate the accumulation of lipid peroxidation as described previously [19] (Fig. 3J-M). Furthermore, xCT activity was inhibited by DSF/Cu, as evidenced by the reduced extracellular cystine pool (Fig. S5F). Collectively, these findings indicated that DSF/Cu induced both ferroptosis and cuproptosis, which is accompanied by the depletion of GSH, elevation of lipid peroxides, and compensatory elevation of xCT.

3.4. DSF/Cu increases xCT expression by inhibiting the ubiquitination–proteasome degradation

Previous research demonstrated that ATF4 promotes the expression of xCT via the transcriptional-dependent mechanism [48]. Therefore, we wonder whether the increased ATF4 is responsible for the compensatory elevation of xCT. To test this hypothesis, the expression of ATF4 in two HCC cell lines was silenced. Indeed, we found that the knockdown of ATF4 facilitated the DSF/Cu-induced cell death and exacerbated the generation of lipid peroxides under the challenge of DSF/Cu (Fig. 4A–F and Fig. S6). ATF4 knockdown was unable to block the compensatory elevation of xCT and the GSH reduction (Fig. 4G–K). Additionally, the quantitative PCR analysis manifested that the mRNA of *ATF4* was markedly increased, while the expression of *xCT* dramatically declined under the treatment of DSF/Cu, demonstrating that a post-transcriptional mechanism involves the compensatory elevation of xCT (Fig. 5A–D). We next focused on the ubiquitination–proteasome degradation pathway. The toxicity of DSF/Cu could be aggravated in cycloheximide (CHX, a chemical protein synthesis inhibitor) pretreatment cells (Fig. 5E–F and Fig. S7). Meanwhile, the western blot showed that CHX dramatically limited the DSF/Cu-induced elevated ATF4 but did not significantly abrogate the increased expression of xCT. Conversely, MG132 (a proteasome inhibitor) augmented the compensatory increase of xCT under exposure to DSF/Cu (Fig. 5G and H). Following this, the half-life of xCT protein under the pre-treatment of protein synthase inhibitor cycloheximide was next measured. Results illustrated that DSF/Cu substantially dampened the degradation of xCT (Fig. 5I). The ubiquitin-proteasome system serves as the primary mechanism for protein degradation in cells [49]. However, further study indicated that the ubiquitination level exhibited an increasing trend with increased DSF/Cu concentrations, which was further augmented by MG132 and inhibited by CHX (Fig. 5J and K). This indicated that DSF/Cu treatment induces phenotypic characteristics similar to those observed with proteasome inhibitors, as it stabilizes ubiquitylated proteins by interfering with the upstream of ubiquitin-proteasome system, thus inducing the accumulation of ubiquitinated protein. Specifically, the Huh7 cell line with stable over-expression of xCT was constructed and Co-IP assay was performed to detect the ubiquitination of xCT. As shown in Fig. 5L, M with the treatment of DSF/Cu, the ubiquitination of xCT was elevated, demonstrating that the degradation of xCT was blocked. In conclusion, these results implied that DSF/Cu inhibited ubiquitination-mediated proteasomal degradation of xCT protein, which eventually led to the accumulation of xCT protein.

3.5. Inhibition of xCT renders the sensitivity to DSF/Cu-induced cell death

To know whether repressing the compensatory increase of xCT could endow DSF/Cu with enhanced toxicity on HCC cells, SASP and erastin (two wildly used xCT inhibitors) were selected for further verification. The cell viability, Calcein-AM/PI assay and clonogenic cell survival showed that pharmacological inhibition of xCT promoted the DSF/Cu-induced cell death and eliminated the live cells (Fig. 6A–D and Fig. S8). In addition, the results from the laser confocal microscope revealed that SASP and erastin increased the accumulation of lipid

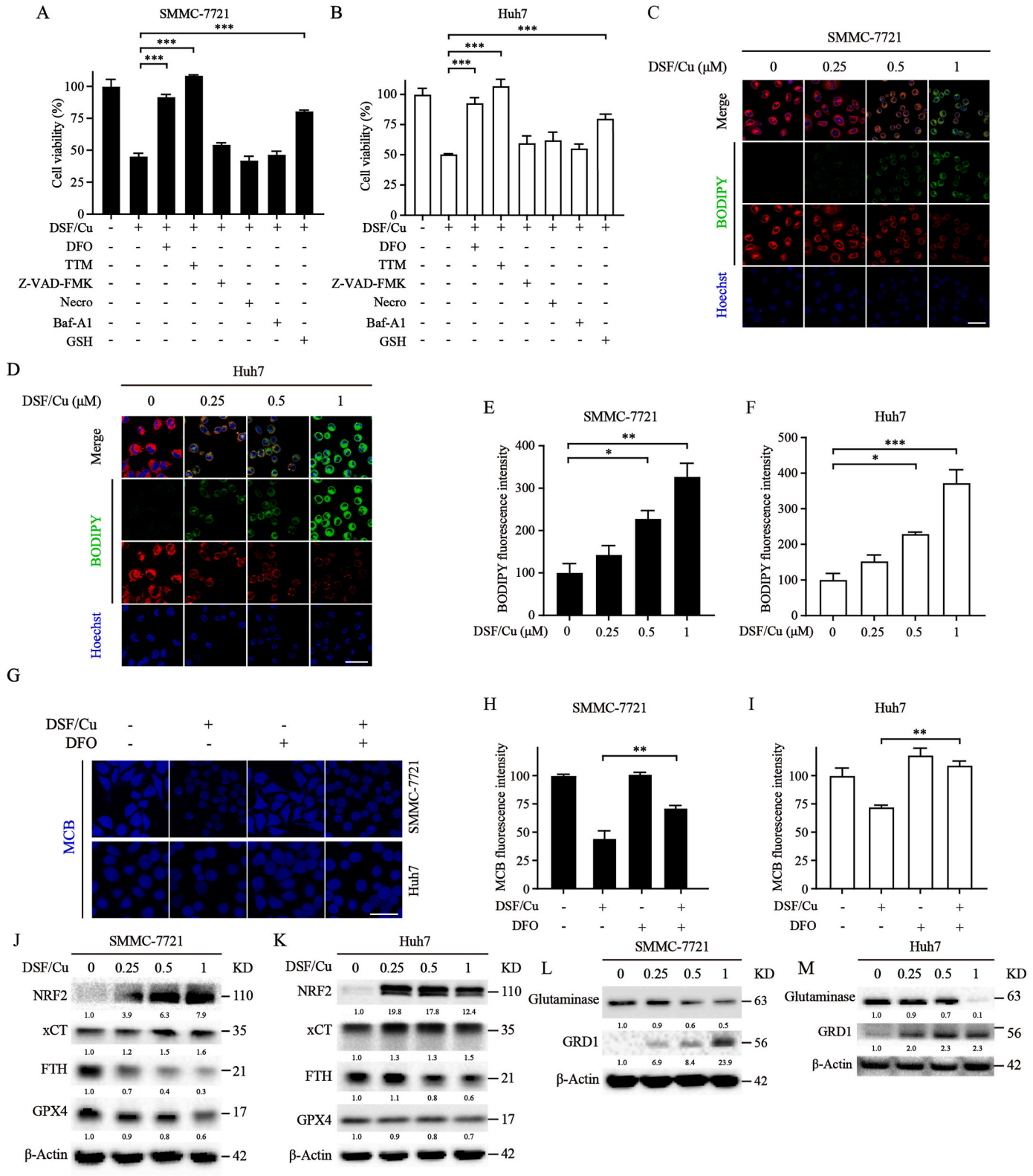

Fig. 3. DSF/Cu induces ferroptosis and compensatorily activates cellular xCT levels in HCC cells
SMMC-7721 (A) and Huh7 (B) were treated with DSF/Cu (0.5 μM) for 12 h under the presence or absence of various small molecular inhibitors, DFO (100 μM), TTM (10 μM), Z-VAD- FMK (1 μM), Necro (1 μM), Baf-A1 (20 nM), and GSH (1 mM). (C, D) Confocal microscopy images revealed the variation of lipid peroxidation stained by BODIPY probe (4 μM) in two HCC cell lines. Scale bar: 50 μm. (E, F) The quantitative histograms of (C) and (D). (G) The level of intracellular GSH was determined by MCB staining (25 μM) after incubating with DSF/Cu (0.5 μM) for 6 h with or without DFO (100 μM) pretreatment in SMMC-7721 and Huh7 cells. Scale bar: 50 μm. The fluorescence was quantitative in (H) and (I). (J, K) The expression of NRF2, xCT, FTH, and GPX4 proteins was analyzed by western blot. (L, M) The GSH metabolism-related proteins were explored by western blot. β-Actin served as the reference housekeeping gene. (Compared with control or between groups, * indicated $P < 0.05$, ** indicated $P < 0.01$, and *** indicated $P < 0.001$).

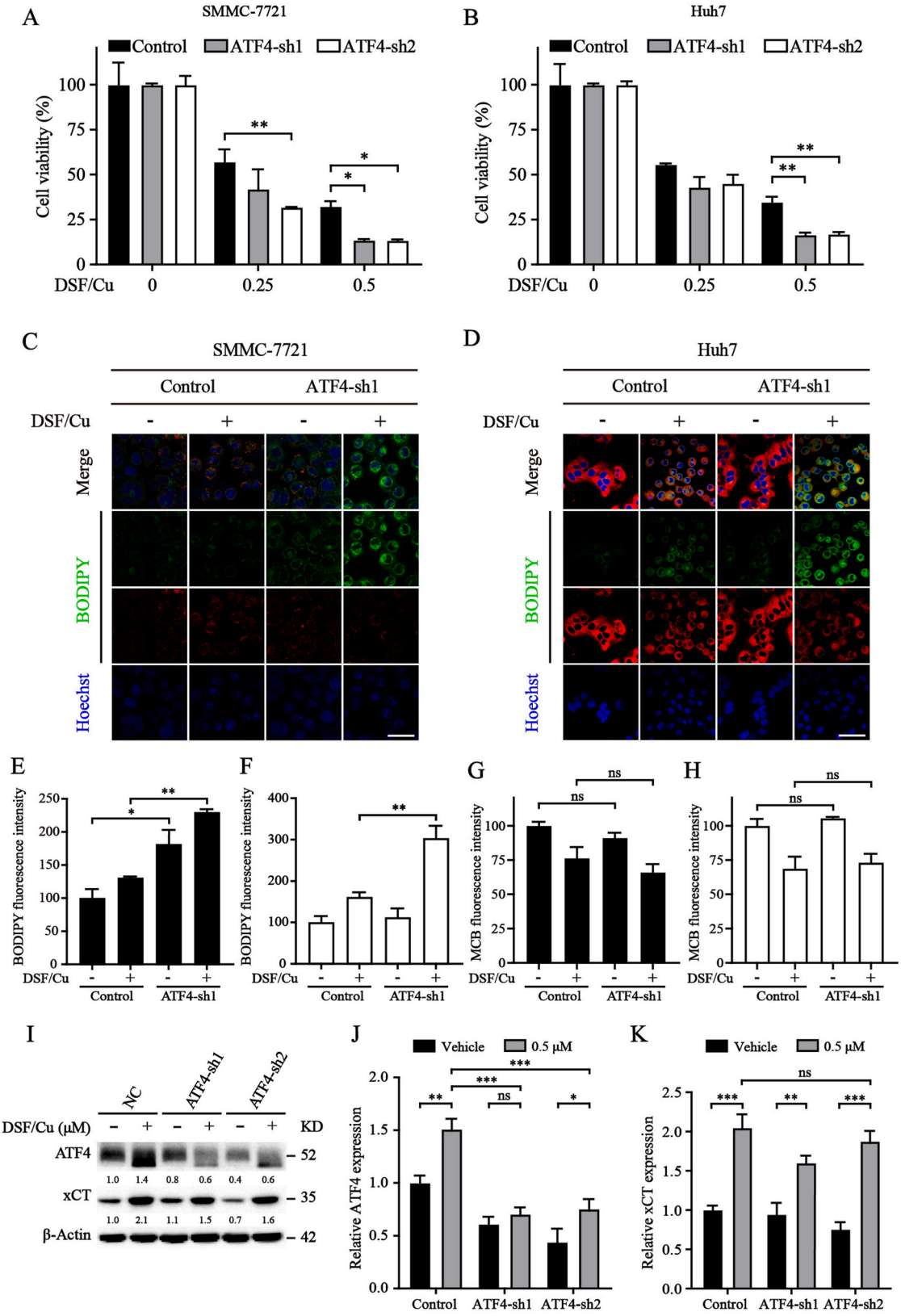

Fig. 4. Inhibition of ATF4 promotes the sensitivity of DSF/Cu-induced ferroptosis

(A, B) Cell viability of control, ATF4-sh1, and ATF4-sh2 SMMC-7721 and Huh7 were detected under the treatment of DSF/Cu with different concentrations. (C, D) Control and ATF4-sh1 of SMMC-7721 and Huh7 were incubated with or without DSF/Cu (0.25 μM) for 6 h and stained for BODIPY (4 μM) and Hoechst (1 μg/mL), then photographed by a confocal laser microscope and quantitated on histograms (E) and (F), respectively. Scale bar: 50 μm. (G, H) The level of intracellular GSH was determined by MCB staining (25 μM) in control and ATF4-sh1 of SMMC-7721 and Huh7 cells. (I–K) After the cells were exposed to DSF/Cu (0.5 μM) or not for 12 h, western blot was utilized to measure the protein expression in SMMC-7721 and the quantitative histograms were displayed on the right. β-Actin was used as a loading control. (Compared with control, * indicated $P < 0.05$ and ** indicated $P < 0.01$).

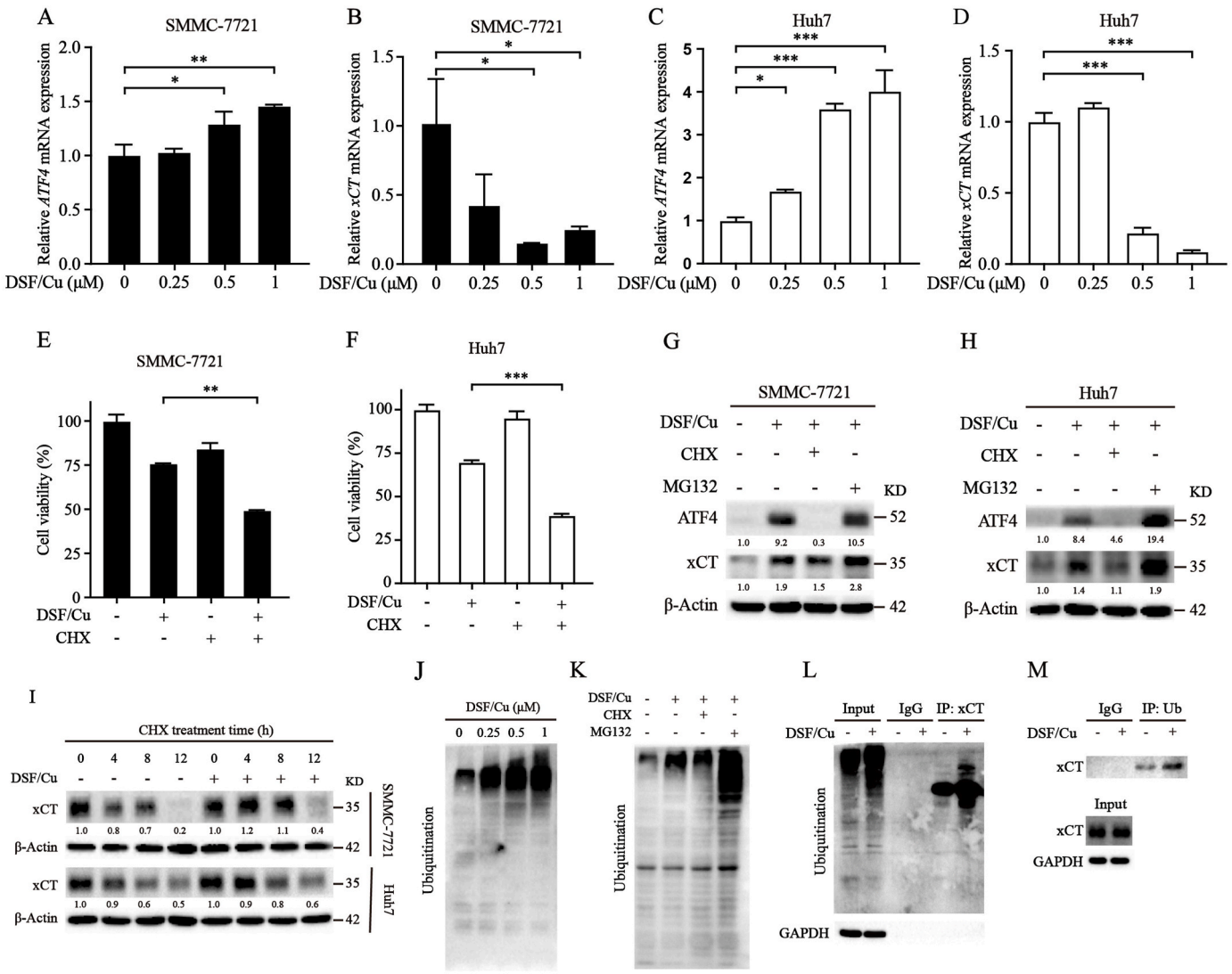

Fig. 5. DSF/Cu increases xCT expression by inhibiting the ubiquitination–proteasome degradation
(A-D) Real-time PCR analyzed the relative *ATF4* and *xCT* mRNA levels in DSF/Cu (0–1 μM) treated SMMC-7721 and Huh7 for 12 h. (E, F) The cell viability of HCC cells treated by DSF/Cu (0.5 μM) combined with 100 μg/mL CHX for 12 h. (G, H) Levels of ATF4 and xCT were determined by western blot with the indicated treatment. (I) Western blot explored the expression of xCT after HCC cells were treated with 100 μg/mL CHX with or without 0.5 μM DSF/Cu at different times. (J, K) The ubiquitinated proteins were determined in Huh7 cells by western blot with the indicated treatment. (L–M) The ubiquitination of xCT protein was detected by Co-IP in xCT over-expression Huh7 cells. (Compared with control, * indicated $P < 0.05$, ** indicated $P < 0.01$, and *** indicated $P < 0.001$).

peroxidation and reduced the cellular GSH levels (Fig. 6E–J), indicating that the pharmacological inhibition of xCT had a promoting effect on the DSF/Cu-induced ferroptosis. To further identify the effect, the cells with xCT knockdown were constructed. First of all, the cell viabilities and clonogenic cell survival were determined and the results showed that xCT knockdown inhibited the cell viability, which could be recovered by GSH (Fig. 7A and B and Fig. S9). Furthermore, the lipid peroxides were significantly increased and the GSH level was substantially reduced in the xCT-silenced cells (Fig. 7C–I). In summary, these data confirmed that inhibiting the compensatory increase of xCT renders HCC cells more susceptible to DSF/Cu-mediated cell death.

3.6. *DSF/Cu treatment suppresses tumor growth in vivo*

To explore the therapeutic effect of DSF/Cu on HCC *in vivo*, the subcutaneous tumor models were constructed with Huh7 cells. Treatment with DSF/Cu effectively suppressed tumor growth, as evidenced by a significant reduction in tumor volume compared to the control group (Fig. 8A and B). Clinical application requires the security of the drug and the toxicity of DSF/Cu was one of the major concerns. As shown in Fig. 8C, biochemical markers of liver and kidney functions were examined and DSF/Cu did not adversely affect the detected markers. The pathological evaluation of HE staining showed that treatment of DSF/Cu did not affect the pathological morphology of liver and kidney tissues, indicating the high security and tolerance of DSF/Cu (Fig. 8D). Consistent with the *in vitro* findings, the immunohistochemistry staining and western blot analysis demonstrated that treatment of DSF/Cu promoted the expression of xCT, HSP70 and ATF4, with the suppression of Ki-67 (Fig. 8E–G). Additionally, the administration of DSF/Cu led to the excessive accumulation of lipid peroxide and a decrease in GSH (Fig. 8H). Collectively, Our findings show that DSF/Cu is not only tolerable but also beneficial, which may act as a promising therapy for treating hepatocellular carcinoma.

4. Discussion

HCC is one of the most widespread malignant cancers in the world and is usually detected at an advanced stage [50]. Late diagnosis and

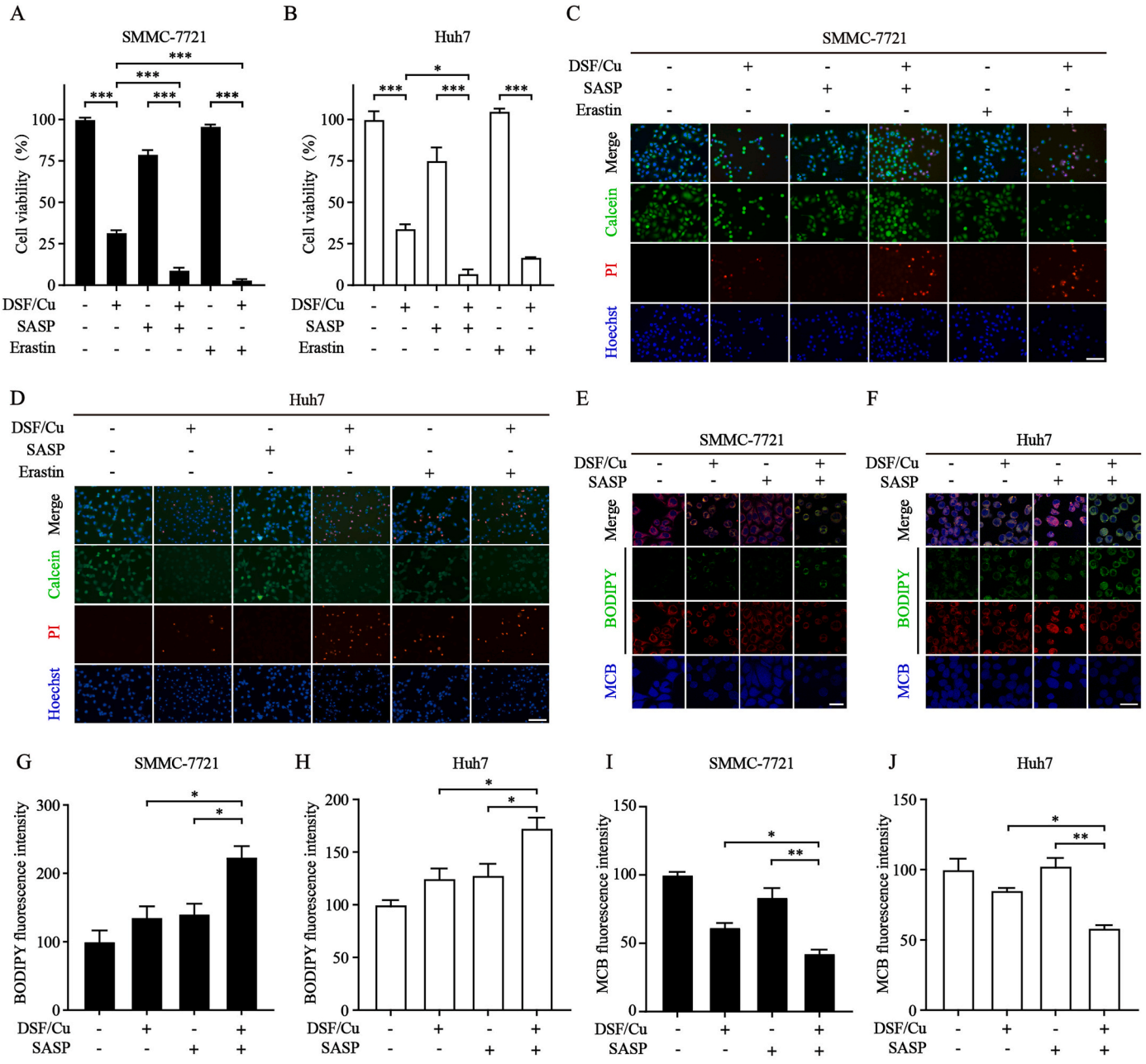

Fig. 6. Pharmacologic suppression of xCT facilitates the DSF/Cu-induced ferroptosis in HCC cells
(A, B) The cell viability of SMMC-7721 (A) and Huh7 (B) cells was assessed under the existence or absence of xCT inhibitors for 12 h. (C, D) Fluorescence staining of Calcein/PI detected live/dead cells. SMMC-7721 and Huh7 were treated with DSF/Cu (0.25 μM), erastin (10 μM), SASP (1 mM), and in combination for 12 h. Scale bar: 200 μm. (E–J) BODIPY (4 μM) and MCB (25 μM) were performed to determine lipid peroxidation and GSH levels in SMMC-7721 and Huh7, which were exposed to DSF/Cu (0.25 μM) and SASP (1 mM) in combination or alone for 6 h. Scale bar: 50 μm. Quantitative for the level of lipid peroxidation and GSH in SMMC-7721 and Huh7 cells were displayed in G-J. (Compared with control or between groups, * indicated $P < 0.05$, and ** indicated $P < 0.01$).

treatment complications have a profound impact on the prognosis of patients with HCC, significantly influencing their overall outcomes. The increasing morbidity and mortality of HCC pose significant challenges to public health. It is noteworthy that the liver plays a crucial role in regulating iron metabolism and maintaining iron homeostasis in the body. This function is carried out through the production and secretion of hepcidin, a key regulator of iron levels [51]. Hepatocytes obtain iron through TFR1 and SLC39A14 and export it through FPN [52]. Based on the importance of the liver to iron metabolism, more research showed that HCC is susceptible to ferroptosis [52]. Ferroptosis is a novel discovered form of controlled cell death characterized by lipid peroxidation, which major depends on the regulation of GSH and iron [53,54]. GSH, as a substrate for GPX4, possesses the ability to inhibit ferroptosis by reducing lipid peroxides [55]. Meanwhile, an imbalance of iron metabolism could result in the accumulation of iron-based lipid peroxides [56].

DSF has been employed for the treatment of alcoholism for more than 7 decades with proven safety [57]. At present, there is an increasing amount of evidence suggesting that the metabolites of DSF could be combined with copper ions to form CuET complexes and exert excellent anti-cancer function [58]. CuET is capable of bypassing the copper transporter system and selectively releasing cupric ions under the action of ROS. Such conditions may exist in cancer cells that are often under oxidative stress, making tumor tissue much more sensitive to the

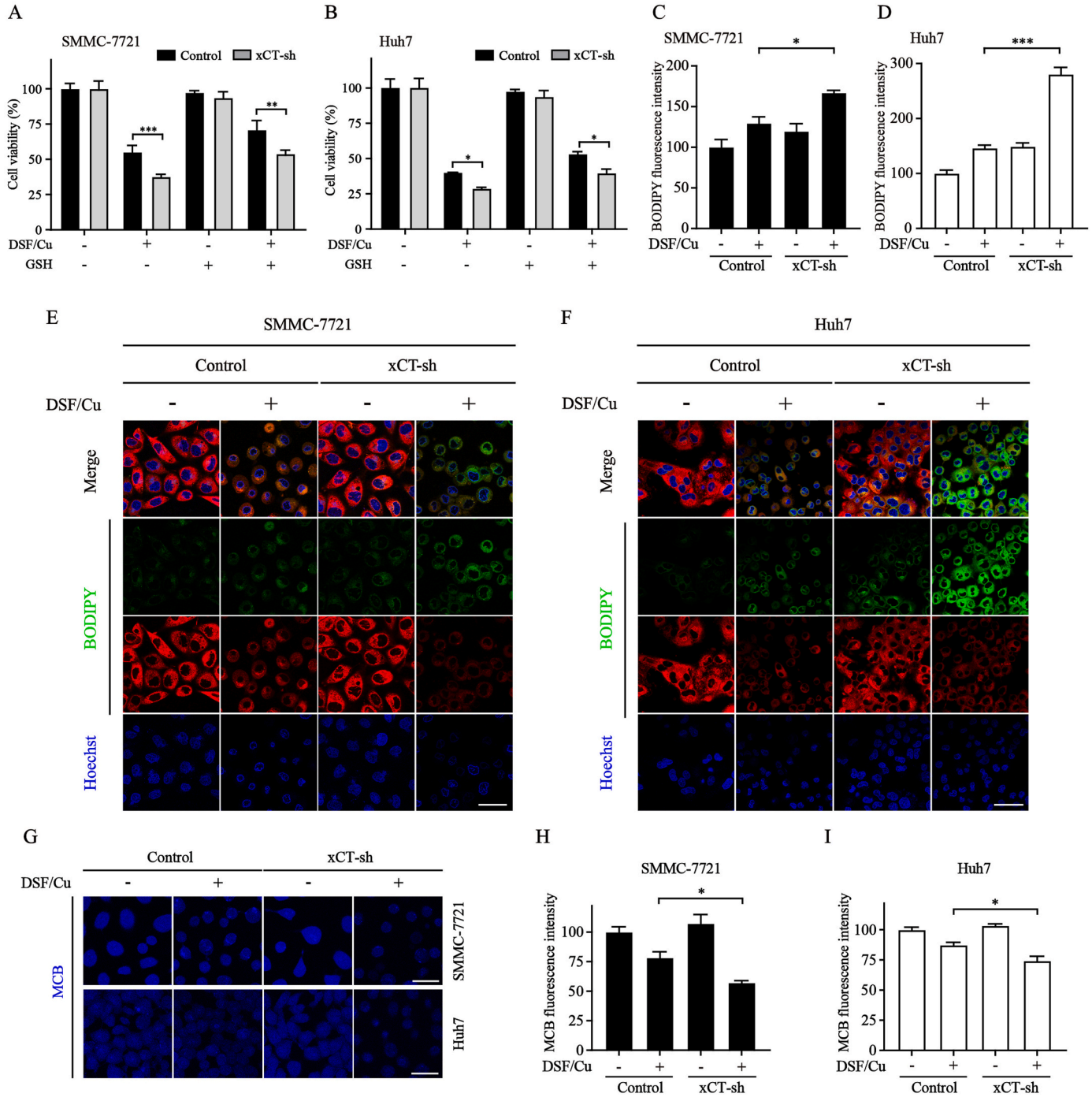

Fig. 7. Knockdown of xCT renders the sensitivity to DSF/Cu-induced ferroptosis in HCC cells
(A, B) CCK-8 assay was performed after the cells with indicated treatment for 12 h. (C–F) Lipid peroxides were examined by BODIPY (4 μM) staining in HCC cells incubated with DSF/Cu (0.25 μM) for 6 h. Scale bars: 50 μm. (G–I) HCC cells were stained with an MCB probe (25 μM) and the image was captured by a laser microscope. The statistical histograms were displayed on the right. Scale bars: 50 μm (Compared with control or between groups, * indicated $P < 0.05$, and ** indicated $P < 0.01$).

DSF/Cu-induced programmed cell death [59]. *Hubert et al.* found DSF/Cu treatment caused a>20-fold increase in cellular Cu of NSCLC patients and DSF toxicity was shown to be dependent on the retention of Cu as well as oxidative stress [60]. The currently known mechanism of anti-cancer for DSF/Cu includes the following: disrupting proteasome activity [61], inhibiting NF-kB/BCL6 signaling pathways [62], targeting p97-Npl4 complex [63], suppressing DNMT activity [64] and inducing diverse programmed cell death. It is noteworthy that many cellular signaling pathways may be affected by DSF/Cu. In our investigation, we found DSF/Cu could induce both cuproptosis and ferroptosis in HCC cells to achieve the anti-cancer effect.

In the current study, we found that DSF/Cu treatment triggered ER stress as evidenced by dilated morphology of ER and disrupted calcium homeostasis, with the up-regulated ATF4, HSP70, CHOP, and p-eIF2α in DSF/Cu-treated HCC cells. Pharmacologic inhibition of ER stress or silencing of ATF4 contributes to the tolerance of DSF/Cu, suggesting ER stress may be a protective mechanism activated by HCC cells to reduce DSF/Cu-caused toxicity. A previous study reported that the

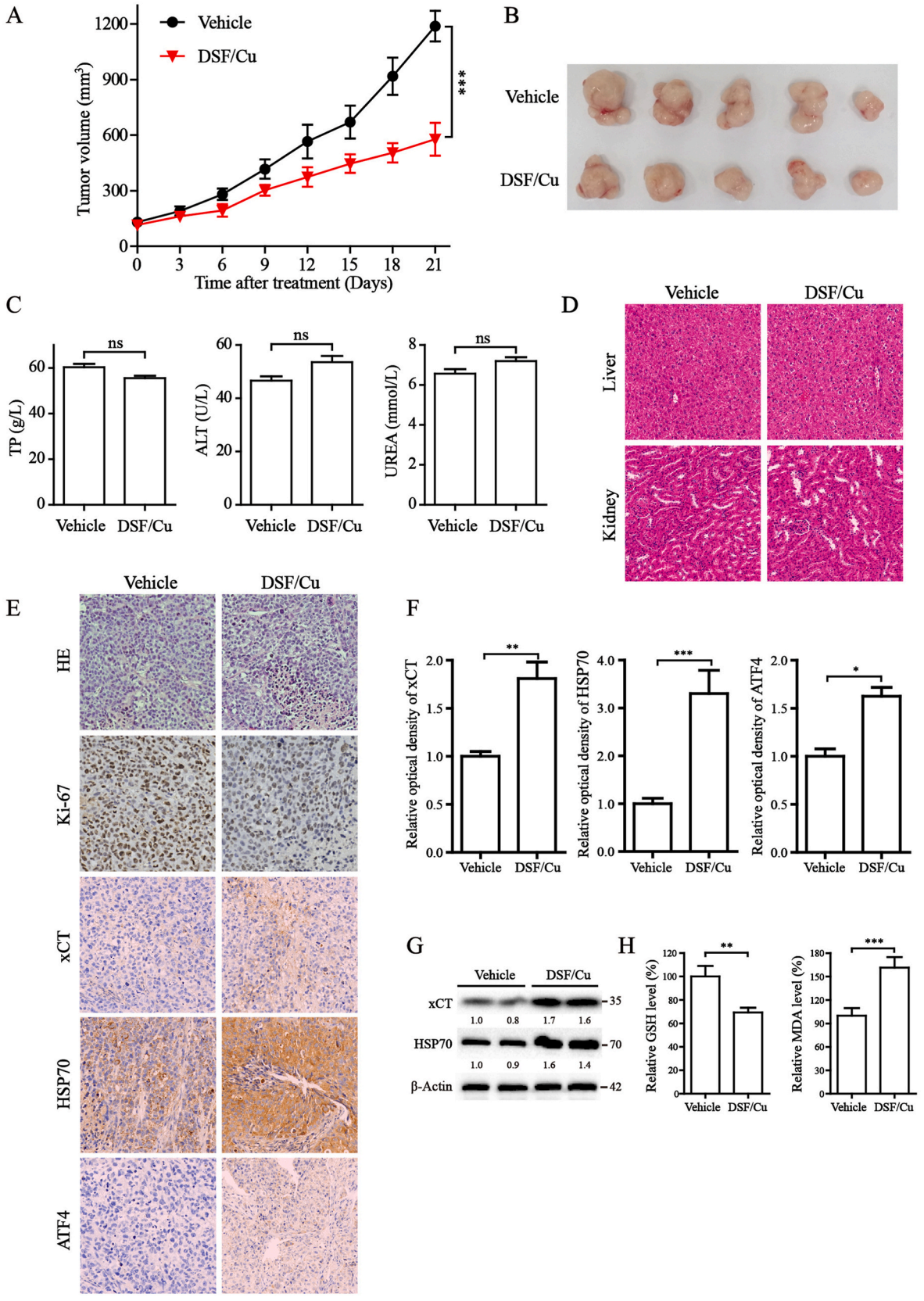

Fig. 8. The treatment of DSF/Cu suppresses tumor growth *in vivo*
(A, B) The animal models were established and randomly divided into control and DSF/Cu treatment group. The tumor volume was determined every 3 days. (C, D) Analysis of liver and kidney functions, through blood routine examination and H&E staining. (E) H&E staining and IHC analysis of Ki-67, xCT, HSP70, ATF4 in indicated tumor specimens. (F) The quantitative histograms of the IHC staining. (G) The western blot analysis of tumor tissues. (H) The relative GSH and MDA levels in tumor tissues.

physiological activity of xCT (also known as SLC7A11, x Solute carrier family 7 members 11) could be transcriptional activated by ATF4, a responsive target in ER stress [48]. Exactly, it has been discovered in this work that the expression of ATF4 was up-regulated accompanied by DSF/Cu-induced ER stress. Meanwhile, the knockdown of ATF4 facilitated the DSF/Cu-induced cell death and exacerbated the generation of lipid peroxides under the challenge of DSF/Cu. However, ATF4 knockdown was unable to block the compensatory elevation of xCT, indicating compensatory elevating of xCT expression was not transcription-dependent. Recent research has demonstrated that the metabolic derivative of disulfiram, CuET, could inhibit cancer cells by targeting the p97-Npl4 complex and subsequently abrogated the ubiquitination–proteasome mediated degradation [63,65]. Further biochemical and structural investigation revealed that cupric ions may be released from CuET under oxidative conditions and thus interact with the zinc finger motifs of Npl4, leading to the inactive of p97 through a conformational lock [59]. Similarly, in our current study, we found that DSF/Cu induced the accumulation of ubiquitinated proteins, promoted the half-life of xCT protein, and dramatically dampened the ubiquitination–proteasome mediated degradation of xCT.

The liver possesses a high content of GSH in the human body, which plays a crucial role in effectively reducing lipid peroxide levels when faced with the challenge of ferroptosis [66,67]. High concentration of GSH could contribute to drug resistance by enhancing the ability to inhibit lipid peroxidation and ferroptosis through its strong reducibility [68]. It is generally accepted that xCT can promote the synthesis of GSH for ferroptosis inhibition, which may be a resistance mechanism of DSF/Cu in cancer therapy [69]. In our investigation, it was discovered that DSF/Cu could induce ferroptosis by increased lipid peroxides and decreased GSH *in vivo* and *in vitro*. Moreover, both pharmacologically and genetically suppressing xCT exacerbated DSF/Cu-induced cell death. These findings imply that suppressing the compensatory upregulation of xCT could facilitate DSF/Cu-mediated ferroptosis, which may enhance the therapeutic efficacy of DSF/Cu and potentially reduce the resistance of HCC cells to DSF/Cu. A previous study also demonstrated that DSF was shown to selectively enhance radiation and chemotherapy-induced NSCLC killing and reduce radiation and chemotherapy resistance in hypoxia [60]. Similar to the results, our early study revealed that DSF/Cu could strengthen the cytotoxicity of sorafenib, and arrest tumor growth both *in vitro* and *in vivo*, by simultaneously inhibiting the signal pathway of NRF2 and MAPK kinase [42]. This provides a theoretical foundation for the clinical application of DSF/Cu in cancer therapy.

Cuproptosis is a recently discovered new form of programmed cell death that is dependent on mitochondrial respiration and characterized by lipoylated protein aggregation and iron-sulfur cluster protein loss [45]. FDX1 and lipoylated protein are abundant in a diversity of human tumors, and cancer cells with high mitochondrial respiration metabolic profiles are sensitive to copper ionophore-mediated cuproptosis [70]. In HCC, high expression of FDX1 was associated with longer survival time [71]. For tumors with such metabolic characteristics, copper ion carrier therapy provides a new and challenging research direction. In the current work, DSF/Cu significantly initiated cuproptosis with down-regulation of iron-sulfur proteins and FDX1. Our recent paper demonstrated that human ISCA1, ISCA2 and ISCU proteins harbor strong copper-binding activity, which would impair Fe–S assembly [72]. These observations may be the potential mechanism for the reduced iron-sulfur proteins in the process of cuproptosis.

Tumor suppressor gene p53 can be activated by various stress signals, resulting in the formation of polymers when combined with DNA, which is involved in the regulation of gene transcription [73]. P53 can activate several metabolic genes to enhance GSH biosynthesis, in order to protect the cell from oxidative toxicity [74]. Interestingly, it has been shown that p53 can inhibit the transcription of xCT, restrain the synthesis of GSH, and aggravate the degree of ferroptosis [75]. Our study found that GSH is the intersection of ferroptosis and cuproptosis, suggesting that p53 may also regulate cuproptosis through the GSH pathway. Through experimentation using p53 wild-type SMMC-7721 cells and p53 mutant huh7 cells, it was observed that under low concentrations of DSF/Cu, the xCT transcript level and GSH level decreased more significantly in SMMC-7721 cells. This decrease may be attributed to the activation of p53. However, there was no significant difference in the toxicity of DSF/Cu between the two cell types, suggesting that further investigation is required to determine the potential role of p53 pathway in the mechanisms of DSF/Cu-mediated cell death.

In conclusion, the current work provides an in-depth study on the mechanism of DSF/Cu-induced cell death and describes a framework for the further understanding of the crosstalk between ferroptosis and cuproptosis. Notable, inhibiting the compensatory increase of xCT renders HCC cells more susceptible to DSF/Cu, which may provide a promising synergistic strategy to sensitize tumor therapy and overcome drug resistance, as it activates different programmed cell death.

Ethics approval and consent to participate

Animal experiments were performed in strict adherence to the relevant guidelines and regulations of the Animal Care and Use Committee of the Zhejiang Provincial People's Hospital and approved by the Animal Ethics Committee of the Zhejiang Provincial People's Hospital (approval number A202100027).

Availability of data and materials

All data generated during this study are included either in this article or in additional files.

Consent for publication

Not applicable.

Funding

This research was supported by National Natural Science Foundation of China (Nos. 82202429, 82102938); Zhejiang Provincial Natural Science Foundation of China (Nos. LBY23H080004, LBY23H080005, LBY23H080001). Medical and Health Science and Technology Project of Zhejiang Province (Grant Nos. 2023RC228, 2023RC004, 2022KY236, 2022KY074).

CRediT authorship contribution statement

Ping Zhang: Investigation, Validation, Visualization, Writing – original draft. **Chaoting Zhou:** Software, Validation, Visualization, Writing – review & editing. **Xueying Ren:** Conceptualization, Investigation, Methodology, Software, Validation. **Qiangan Jing:** Conceptualization, Investigation, Methodology. **Yan Gao:** Software, Validation. **Chen Yang:** Investigation, Methodology. **Yuhuan Shen:** Resources, Software, Validation. **Yi Zhou:** Formal analysis. **Wanye Hu:** Resources, Software. **Feifan Jin:** Data curation. **Haifeng Xu:** Software, Validation. **Lingyan Yu:** Formal analysis, Investigation. **Yingchao Liu:** Software. **Xiangmin Tong:** Supervision. **Yanchun Li:** Supervision, Writing – review & editing. **Ying Wang:** Supervision, Writing – review & editing. **Jing Du:** Supervision, Writing – review & editing.

Declaration of competing interest

The authors declare that they have no known competing financial interests or personal relationships that could have appeared to influence the work reported in this paper.

Data availability

Data will be made available on request.

Acknowledgments

Not applicable.

List of abbreviations

HCC	hepatocellular carcinoma
DSF	disulfiram
FDA	food and drug administration
DTC	diethyldithiocarbamate
ER	endoplasmic reticulum
NF-κB	nuclear factor kappa-B
TGF-β	transforming growth factor beta
GPX4	glutathione peroxidase 4
GSH	glutathione
NRF2	nuclear factor erythroid 2-related factor 2
FSP1	ferroptosis suppressor protein 1
ATF4	recombinant activating transcription factor 4
xCT x	Solute carrier family 7 members 11
GluT1	glucose transporter 1
GRD1	recombinant glutathione reductase 1
eIF2α	eukaryotic translation initiation factor 2 subunit alpha
HSP70	heat shock protein 70
CHOP	C/EBP homologous protein
FTH	ferritin heavy chain
TFR1	transferrin receptor 1
SLC39A14	solute carrier family 39 (zinc transporter), member 14
BCL6	B celll ymphoma 6
NPL4	ubiquitin recognition factor
UPR	unfolded protein response
PERK	PKR-like endoplasmic reticulum kinase
PUMA	53 Up-regulated modulator of apoptosis
NFS1	nitrogen fixation 1
CISD3	CDGSH iron-sulfur domain-containing protein 3
NDUFV2	NADH dehydrogenase (ubiquinone) flavoprotein 2
FDX1	ferredoxin 1

Appendix A. Supplementary data

Supplementary data to this article can be found online at https://doi.org/10.1016/j.redox.2023.103007.

References

[1] F. Bray, J. Ferlay, I. Soerjomataram, R.L. Siegel, L.A. Torre, A. Jemal, Global cancer statistics 2018: GLOBOCAN estimates of incidence and mortality worldwide for 36 cancers in 185 countries, Ca-Cancer J. Clin. 68 (6) (2018) 394–424.
[2] L. Rahib, M.R. Wehner, L.M. Matrisian, K.T. Nead, Estimated projection of US cancer incidence and death to 2040, JAMA Netw. Open 4 (4) (2021), e214708.
[3] A.B. Benson, M.I. D'Angelica, D.E. Abbott, D.A. Anaya, S.D. Darlow, Hepatobiliary cancers, version 2.2021, NCCN clinical practice guidelines in oncology, J. Natl. Compr. Cancer Netw.: J. Natl. Compr. Cancer Netw. 19 (5) (2021) 541–565.
[4] Chen CY. Chemotherapeutic drug-regulated cytokines might influence therapeutic efficacy in HCC. Int. J. Mol. Sci., 22(24): 13627.
[5] J.M. Llovet, S. Ricci, V. Mazzaferro, P. Hilgard, J. Bruix, SHARP Investigators Study Group. Sorafenib in advanced hepatocellular carcinoma, N. Engl. J. Med. 359 (4) (2008) 378–390.
[6] L. Wei, D. Lee, C.-T. Law, M.S. Zhang, J. Shen, D.W.-C. Chin, et al., Genome-wide CRISPR/Cas9 library screening identified PHGDH as a critical driver for Sorafenib resistance in HCC, Nat. Commun. 10 (1) (2019) 4681.
[7] B. Sangro, P. Sarobe, S. Hervás-Stubbs, I. Melero, Advances in immunotherapy for hepatocellular carcinoma, Nat. Rev. Gastroenterol. Hepatol. 18 (8) (2021) 525–543.
[8] S. Pushpakom, F. Iorio, P.A. Eyers, K.J. Escott, S. Hopper, A. Wells, et al., Drug repurposing: progress, challenges and recommendations, Nat. Rev. Drug Discov. 18 (1) (2019) 41–58.
[9] S. Zhong, L. Shengyu, S. Xin, X. Zhang, K. Li, G. Liu, et al., Disulfiram in glioma: literature review of drug repurposing, Front. Pharmacol. 13 (2022), 933655.
[10] H. Li, J. Wang, C. Wu, L. Wang, Z.-S. Chen, W. Cui, The combination of disulfiram and copper for cancer treatment, Drug Discov. Today 25 (6) (2020) 1099–1108.
[11] H. Shi, Y. Suo, Z. Zhang, R. Liu, H. Liu, Z. Cheng, Copper(II)-disulfiram loaded melanin-dots for cancer theranostics, Nanomed. Nanotechnol. Biol. Med. 32 (2021), 102340.
[12] V.T. Cheriyan, Y. Wang, M. Muthu, S. Jamal, D. Chen, H. Yang, et al., Disulfiram suppresses growth of the malignant pleural mesothelioma cells in part by inducing apoptosis, PLoS One 9 (2014).
[13] S. Karanam, S. Sharma, R. Chowdhury, A. Roy, Disulfiram potentiates docetaxel cytotoxicity in breast cancer cells through enhanced ROS and autophagy, Pharmacol. Rep.: PR (Suppl 2) (2020).
[14] X. Wu, X. Xue, L. Wang, W. Wang, J. Han, X. Sun, et al., Suppressing autophagy enhances disulfiram/copper-induced apoptosis in non-small cell lung cancer, Eur. J. Pharmacol. 827 (2018) 1.
[15] R. Xu, K. Zhang, J. Liang, F. Gao, F. Guan, Hyaluronic acid/polyethyleneimine nanoparticles loaded with copper ion and disulfiram for esophageal cancer, Carbohydr. Polym. 261 (9687) (2021), 117846.
[16] Y. Kao, L.C. Huang, S.Y. Hsu, S.M. Huang, D.Y. Hueng, The effect of disulfiram and copper on cellular viability, ER stress and ALDH expression of human meningioma cells, Biomedicines 10 (4) (2022).
[17] Jie Z, Sb C, Mda B, Kai CD, Ps E, Lfa B, et al. Disulfiram/copper Shows Potent Cytotoxic Effects on Myelodysplastic Syndromes via Inducing Bip-Mediated Apoptosis and Suppressing Autophagy - ScienceDirect.
[18] Y. Li, L.H. Wang, H.T. Zhang, Y.T. Wang, S. Liu, W.L. Zhou, et al., Disulfiram combined with copper inhibits metastasis and epithelial-mesenchymal transition in hepatocellular carcinoma through the NF-κB and TGF-β pathways, J. Cell Mol. Med. 22 (1) (2018) 439–451.
[19] X. Ren, Y. Li, Y. Zhou, W. Hu, C. Yang, Q. Jing, et al., Overcoming the compensatory elevation of NRF2 renders hepatocellular carcinoma cells more vulnerable to disulfiram/copper-induced ferroptosis, Redox Biol. 46 (2021), 102122.
[20] B.R. Stockwell, Ferroptosis turns 10: emerging mechanisms, physiological functions, and therapeutic applications, Cell 185 (14) (2022) 2401–2421.
[21] W. Hu, C. Zhou, Q. Jing, Y. Li, J. Yang, C. Yang, et al., FTH promotes the proliferation and renders the HCC cells specifically resist to ferroptosis by maintaining iron homeostasis, Cancer Cell Int. 21 (1) (2021) 709.
[22] Y. Li, B. Xu, X. Ren, L. Wang, Y. Xu, Y. Zhao, et al., Inhibition of CISD2 promotes ferroptosis through ferritinophagy-mediated ferritin turnover and regulation of p62-Keap1-NRF2 pathway, Cell. Mol. Biol. Lett. 27 (1) (2022) 81.
[23] X. Wang, B. Xu, J. Du, J. Xia, G. Lei, C. Zhou, et al., Characterization of pyruvate metabolism and citric acid cycle patterns predicts response to immunotherapeutic and ferroptosis in gastric cancer, Cancer Cell Int. 22 (1) (2022) 317.
[24] J. Du, X. Wang, Y. Li, X. Ren, Y. Zhou, W. Hu, et al., DHA exhibits synergistic therapeutic efficacy with cisplatin to induce ferroptosis in pancreatic ductal adenocarcinoma via modulation of iron metabolism, Cell Death Dis. 12 (7) (2021) 705.
[25] J. Du, T. Wang, Y. Li, Y. Zhou, X. Wang, X. Yu, et al., DHA inhibits proliferation and induces ferroptosis of leukemia cells through autophagy dependent degradation of ferritin, Free Radic. Biol. Med. 131 (2019) 356–369.
[26] Y. Li, J. Xia, F. Shao, Y. Zhou, J. Yu, H. Wu, et al., Sorafenib induces mitochondrial dysfunction and exhibits synergistic effect with cysteine depletion by promoting HCC cells ferroptosis, Biochem. Biophys. Res. Commun. 534 (2021) 877–884.
[27] C. Zhang, X. Liu, S. Jin, Y. Chen, R. Guo, Ferroptosis in cancer therapy: a novel approach to reversing drug resistance, Mol. Cancer 21 (1) (2022) 47.
[28] F. Yao, Y. Deng, Y. Zhao, Y. Mei, Y. Zhang, X. Liu, et al., A targetable LIFR-NF-κB-LCN2 axis controls liver tumorigenesis and vulnerability to ferroptosis, Nat. Commun. 12 (1) (2021) 7333.
[29] R. Gao, R.K.R. Kalathur, M. Coto-Llerena, C. Ercan, D. Buechel, S. Shuang, et al., YAP/TAZ and ATF4 drive resistance to Sorafenib in hepatocellular carcinoma by preventing ferroptosis, EMBO Mol. Med. 13 (12) (2021), e14351.
[30] R. Iurlaro, C. Muñoz-Pinedo, Cell death induced by endoplasmic reticulum stress, FEBS J. 283 (14) (2016) 2640–2652.
[31] Y. Ma, L.M. Hendershot, The role of the unfolded protein response in tumour development: friend or foe? Nat. Rev. Cancer 4 (12) (2004) 966–977.
[32] M.S. Raab, I. Breitkreutz, G. Tonon, J. Zhang, P.J. Hayden, T. Nguyen, et al., Targeting PKC: a novel role for beta-catenin in ER stress and apoptotic signaling, Blood 113 (7) (2009) 1513–1521.
[33] A.G. Herrmann, R.F. Deighton, T. Le Bihan, M.C. McCulloch, J.L. Searcy, L.E. Kerr, et al., Adaptive changes in the neuronal proteome: mitochondrial energy production, endoplasmic reticulum stress, and ribosomal dysfunction in the cellular response to metabolic stress, J. Cerebr. Blood Flow Metabol. : official journal of the International Society of Cerebral Blood Flow and Metabolism 33 (5) (2013) 673–683.
[34] S.J. Dixon, D.N. Patel, M. Welsch, R. Skouta, E.D. Lee, M. Hayano, et al., Pharmacological inhibition of cystine-glutamate exchange induces endoplasmic reticulum stress and ferroptosis, Elife 3 (2014), e02523.
[35] S. Zhu, Q. Zhang, X. Sun, H.J. Zeh 3rd, M.T. Lotze, R. Kang, et al., HSPA5 regulates ferroptotic cell death in cancer cells, Cancer Res. 77 (8) (2017) 2064–2077.
[36] Y. Chen, Y. Mi, X. Zhang, Q. Ma, Y. Song, L. Zhang, et al., Dihydroartemisinin-induced unfolded protein response feedback attenuates ferroptosis via PERK/ATF4/HSPA5 pathway in glioma cells, J. Exp. Clin. Cancer Res. : CR 38 (1) (2019) 402.
[37] Q. Ru, Y. Li, W. Xie, Y. Ding, L. Chen, G. Xu, et al., Fighting age-related orthopedic diseases: focusing on ferroptosis, Bone research 11 (1) (2023) 12.

[38] E. Merckx, G. Albertini, M. Paterka, C. Jensen, P. Albrecht, M. Dietrich, et al., Absence of system x(c)(-) on immune cells invading the central nervous system alleviates experimental autoimmune encephalitis, J. Neuroinflammation 14 (1) (2017) 9.
[39] F. Shao, Y. Li, W. Hu, J. Yu, H. Wu, K. Ying, et al., Downregulation of CISD2 has prognostic value in non-small cell lung cancer and inhibits the tumorigenesis by inducing mitochondrial dysfunction, Front. Oncol. 10 (2020), 595524.
[40] J. Du, Y. Zhou, Y. Li, J. Xia, Y. Chen, S. Chen, et al., Identification of Frataxin as a regulator of ferroptosis, Redox Biol. 32 (2020), 101483.
[41] X. Yu, X. Wang, X. Wang, Y. Zhou, Y. Li, A. Wang, et al., TEOA inhibits proliferation and induces DNA damage of diffuse large B-cell lymphoma cells through activation of the ROS-dependent p38 MAPK signaling pathway, Front. Pharmacol. 11 (2020), 554736.
[42] X. Ren, Y. Li, Y. Zhou, W. Hu, C. Yang, Q. Jing, et al., Overcoming the compensatory elevation of NRF2 renders hepatocellular carcinoma cells more vulnerable to disulfiram/copper-induced ferroptosis, Redox Biol. 46 (2021), 102122.
[43] X. Chen, J.R. Cubillos-Ruiz, Endoplasmic reticulum stress signals in the tumour and its microenvironment, Nat. Rev. Cancer 21 (2) (2021) 71–88.
[44] L.A. Biwer, B.E. Isakson, Endoplasmic reticulum-mediated signalling in cellular microdomains, Acta Physiol. 219 (1) (2017) 162–175.
[45] P. Tsvetkov, S. Coy, B. Petrova, M. Dreishpoon, A. Verma, M. Abdusamad, et al., Copper induces cell death by targeting lipoylated TCA cycle proteins, Science (New York, NY) 375 (6586) (2022) 1254–1261.
[46] S.C. Lu, Regulation of glutathione synthesis, Mol. Aspect. Med. 30 (1–2) (2009) 42–59.
[47] J. Zhu, M. Berisa, S. Schwörer, W. Qin, J.R. Cross, C.B. Thompson, Transsulfuration activity can support cell growth upon extracellular cysteine limitation, Cell Metabol. 30 (5) (2019) 865–876.
[48] D. Chen, Z. Fan, M. Rauh, M. Buchfelder, I.Y. Eyupoglu, N. Savaskan, ATF4 promotes angiogenesis and neuronal cell death and confers ferroptosis in a xCT-dependent manner, Oncogene 36 (40) (2017) 5593–5608.
[49] D. Nandi, P. Tahiliani, A. Kumar, D. Chandu, The ubiquitin-proteasome system, J. Bio. Sci. 31 (1) (2006) 137–155.
[50] C. Berasain, Inflammation and liver cancer: new molecular links, Ann N Y Acad 1155 (1) (2010) 206–221.
[51] T. Ganz, Hepcidin, a key regulator of iron metabolism and mediator of anemia of inflammation, Blood 102 (3) (2003) 783–788.
[52] J. Chen, X. Li, C. Ge, J. Min, F. Wang, The multifaceted role of ferroptosis in liver disease, Cell Death Differ. 29 (3) (2022) 467–480.
[53] M.M. Gaschler, A.A. Andia, H. Liu, J.M. Csuka, B. Hurlocker, C.A. Vaiana, et al., FINO(2) initiates ferroptosis through GPX4 inactivation and iron oxidation, Nat. Chem. Biol. 14 (5) (2018) 507–515.
[54] Y. Li, X. Wang, Z. Huang, Y. Zhou, J. Xia, W. Hu, et al., CISD3 inhibition drives cystine-deprivation induced ferroptosis, Cell Death Dis. 12 (9) (2021) 839.
[55] X. Jiang, B.R. Stockwell, M. Conrad, Ferroptosis: mechanisms, biology and role in disease, Nat. Rev. Mol. Cell Biol. 22 (4) (2021) 266–282.
[56] Y. Fang, X. Chen, Q. Tan, H. Zhou, J. Xu, Q. Gu, Inhibiting ferroptosis through disrupting the NCOA4-FTH1 interaction: a new mechanism of action, ACS Cent. Sci. 7 (6) (2021) 980–989.
[57] X. Jin, D. Moskophidis, N.F. Mivechi, Heat shock transcription factor 1 is a key determinant of HCC development by regulating hepatic steatosis and metabolic syndrome, Cell Metabol. 14 (1) (2011) 91–103.
[58] X. Peng, Q. Pan, B. Zhang, S. Wan, S. Li, K. Luo, et al., Highly stable, coordinated polymeric nanoparticles loading copper(II) diethyldithiocarbamate for combinational chemo/chemodynamic therapy of cancer, Biomacromolecules 20 (6) (2019) 2372–2383.
[59] M. Pan, Q. Zheng, Y. Yu, H. Ai, Y. Xie, X. Zeng, et al., Seesaw conformations of Npl4 in the human p97 complex and the inhibitory mechanism of a disulfiram derivative, Nat. Commun. 12 (1) (2021) 121.
[60] K.C. Falls-Hubert, A.L. Butler, K. Gui, M. Anderson, M. Li, J.M. Stolwijk, et al., Disulfiram causes selective hypoxic cancer cell toxicity and radio-chemo-sensitization via redox cycling of copper, Free Radic. Biol. Med. (2020) 150.
[61] X. Lun, J.C. Wells, N. Grinshtein, J.C. King, X. Hao, N.H. Dang, et al., Disulfiram when combined with copper enhances the therapeutic effects of temozolomide for the treatment of glioblastoma, Clin. Cancer Res. : an official journal of the American Association for Cancer Research 22 (15) (2016) 3860–3875.
[62] Y. Zhu, C. Lei, Q. Jiang, Q. Yu, L. Qiu, DSF/Cu induces antitumor effect against diffuse large B-cell lymphoma through suppressing NF-κB/BCL6 pathways, Cancer Cell Int. 22 (1) (2022) 236.
[63] Z. Skrott, M. Mistrik, K.K. Andersen, S. Friis, D. Majera, J. Gursky, et al., Alcohol-abuse drug disulfiram targets cancer via p97 segregase adaptor NPL4, Nature 552 (7684) (2017) 194–199.
[64] A.T. Agoston, P. Argani, S. Yegnasubramanian, A.M. De Marzo, M.A. Ansari-Lari, J. L. Hicks, et al., Increased protein stability causes DNA methyltransferase 1 dysregulation in breast cancer, J. Biol. Chem. 280 (18) (2005) 18302–18310.
[65] Z. Skrott, D. Majera, J. Gursky, T. Buchtova, M. Hajduch, M. Mistrik, et al., Disulfiram's anti-cancer activity reflects targeting NPL4, not inhibition of aldehyde dehydrogenase, Oncogene 38 (40) (2019) 6711–6722.
[66] T. Hirschhorn, B.R. Stockwell, The development of the concept of ferroptosis, Free Radic. Biol. Med. 133 (2019) 130–143.
[67] Y. Lin, Y. Li, X. Hu, Z. Liu, J. Chen, Y. Lu, et al., The hepatoprotective role of reduced glutathione and its underlying mechanism in oxaliplatin-induced acute liver injury, Oncol. Lett. 15 (2) (2018) 2266–2272.
[68] L.L. Sun, D.L. Linghu, M.C. Hung, Ferroptosis: a promising target for cancer immunotherapy, Am. J. Cancer Res. 11 (12) (2021) 5856–5863.
[69] Y. Otsuki, J. Yamasaki, K. Suina, S. Okazaki, N. Koike, H. Saya, et al., Vasodilator oxyfedrine inhibits aldehyde metabolism and thereby sensitizes cancer cells to xCT-targeted therapy, Cancer Sci. 111 (1) (2020) 127–136.
[70] D. Luo, S. Liu, J. Luo, H. Chen, Z. He, Z. Gao, et al., Characterization of Cuproptosis Identified Immune Microenvironment and Prognosis in Acute Myeloid Leukemia, Clinical & translational oncology : official publication of the Federation of Spanish Oncology Societies and of the National Cancer Institute of Mexico, 2023.
[71] Z. Zhang, X. Zeng, Y. Wu, Y. Liu, X. Zhang, Z. Song, Cuproptosis-related risk score predicts prognosis and characterizes the tumor microenvironment in hepatocellular carcinoma, Front. Immunol. 13 (2022), 925618.
[72] J. Du, Z. Huang, Y. Li, X. Ren, C. Zhou, R. Liu, et al., Copper exerts cytotoxicity through inhibition of iron-sulfur cluster biogenesis on ISCA1/ISCA2/ISCU assembly proteins, Free Radic. Biol. Med. 204 (2023) 359–373.
[73] S.L. Harris, A.J. Levine, The p53 pathway: positive and negative feedback loops, Oncogene 24 (17) (2005) 2899–2908.
[74] C. Xiong, H. Ling, Q. Hao, X. Zhou, Cuproptosis: p53-regulated metabolic cell death? Cell Death Differ. 30 (4) (2023) 876–884.
[75] L. Jiang, N. Kon, T. Li, S.-J. Wang, T. Su, H. Hibshoosh, et al., Ferroptosis as a p53-mediated activity during tumour suppression, Nature 520 (7545) (2015) 57–62.